

Measurement of the electron charge asymmetry in $p\bar{p} \rightarrow W + X \rightarrow e\nu + X$ events at $\sqrt{s} = 1.96$ TeV

V.M. Abazov³⁶, B. Abbott⁷⁵, M. Abolins⁶⁵, B.S. Acharya²⁹, M. Adams⁵¹, T. Adams⁴⁹, E. Aguilo⁶, M. Ahsan⁵⁹, G.D. Alexeev³⁶, G. Alkhazov⁴⁰, A. Alton^{64,a}, G. Alverson⁶³, G.A. Alves², M. Anastasoaie³⁵, L.S. Ancu³⁵, T. Andeen⁵³, B. Andrieu¹⁷, M.S. Anzelc⁵³, M. Aoki⁵⁰, Y. Arnoud¹⁴, M. Arov⁶⁰, M. Arthaud¹⁸, A. Askew⁴⁹, B. Åsman⁴¹, A.C.S. Assis Jesus³, O. Atramentov⁴⁹, C. Avila⁸, F. Badaud¹³, L. Bagby⁵⁰, B. Baldin⁵⁰, D.V. Bandurin⁵⁹, P. Banerjee²⁹, S. Banerjee²⁹, E. Barberis⁶³, A.-F. Barfuss¹⁵, P. Bargassa⁸⁰, P. Baringer⁵⁸, J. Barreto², J.F. Bartlett⁵⁰, U. Bassler¹⁸, D. Bauer⁴³, S. Beale⁶, A. Bean⁵⁸, M. Begalli³, M. Begel⁷³, C. Belanger-Champagne⁴¹, L. Bellantoni⁵⁰, A. Bellavance⁵⁰, J.A. Benitez⁶⁵, S.B. Beri²⁷, G. Bernardi¹⁷, R. Bernhard²³, I. Bertram⁴², M. Besançon¹⁸, R. Beuselinck⁴³, V.A. Bezzubov³⁹, P.C. Bhat⁵⁰, V. Bhatnagar²⁷, C. Biscarat²⁰, G. Blazey⁵², F. Blekman⁴³, S. Blessing⁴⁹, D. Bloch¹⁹, K. Bloom⁶⁷, A. Boehlein⁵⁰, D. Boline⁶², T.A. Bolton⁵⁹, E.E. Boos³⁸, G. Borissov⁴², T. Bose⁷⁷, A. Brandt⁷⁸, R. Brock⁶⁵, G. Brooijmans⁷⁰, A. Bross⁵⁰, D. Brown⁸¹, X.B. Bu⁷, N.J. Buchanan⁴⁹, D. Buchholz⁵³, M. Buehler⁸¹, V. Buescher²², V. Bunichev³⁸, S. Burdin^{42,b}, T.H. Burnett⁸², C.P. Buszello⁴³, J.M. Butler⁶², P. Calfayan²⁵, S. Calvet¹⁶, J. Cammin⁷¹, E. Carrera⁴⁹, W. Carvalho³, B.C.K. Casey⁵⁰, H. Castilla-Valdez³³, S. Chakrabarti¹⁸, D. Chakraborty⁵², K.M. Chan⁵⁵, A. Chandra⁴⁸, E. Cheu⁴⁵, F. Chevallier¹⁴, D.K. Cho⁶², S. Choi³², B. Choudhary²⁸, L. Christofek⁷⁷, T. Christoudias⁴³, S. Cihangir⁵⁰, D. Claes⁶⁷, J. Clutter⁵⁸, M. Cooke⁵⁰, W.E. Cooper⁵⁰, M. Corcoran⁸⁰, F. Couderc¹⁸, M.-C. Cousinou¹⁵, S. Crépé-Renaudin¹⁴, V. Cuplov⁵⁹, D. Cutts⁷⁷, M. Ćwiok³⁰, H. da Motta², A. Das⁴⁵, G. Davies⁴³, K. De⁷⁸, S.J. de Jong³⁵, E. De La Cruz-Burelo⁶⁴, C. De Oliveira Martins³, J.D. Degenhardt⁶⁴, F. Déliot¹⁸, M. Demarteau⁵⁰, R. Demina⁷¹, D. Denisov⁵⁰, S.P. Denisov³⁹, S. Desai⁵⁰, H.T. Diehl⁵⁰, M. Diesburg⁵⁰, A. Dominguez⁶⁷, H. Dong⁷², T. Dorland⁸², A. Dubey²⁸, L.V. Dudko³⁸, L. Duflot¹⁶, S.R. Dugad²⁹, D. Duggan⁴⁹, A. Duperrin¹⁵, J. Dyer⁶⁵, A. Dyshkant⁵², M. Eads⁶⁷, D. Edmunds⁶⁵, J. Ellison⁴⁸, V.D. Elvira⁵⁰, Y. Enari⁷⁷, S. Eno⁶¹, P. Ermolov^{38,‡}, H. Evans⁵⁴, A. Evdokimov⁷³, V.N. Evdokimov³⁹, A.V. Ferapontov⁵⁹, T. Ferbel⁷¹, F. Fiedler²⁴, F. Filthaut³⁵, W. Fisher⁵⁰, H.E. Fisk⁵⁰, M. Fortner⁵², H. Fox⁴², S. Fu⁵⁰, S. Fuess⁵⁰, T. Gadfort⁷⁰, C.F. Galea³⁵, C. Garcia⁷¹, A. Garcia-Bellido⁸², V. Gavrilov³⁷, P. Gay¹³, W. Geist¹⁹, D. Gelé¹⁹, W. Geng^{15,65}, C.E. Gerber⁵¹, Y. Gershtein⁴⁹, D. Gillberg⁶, G. Ginther⁷¹, N. Gollub⁴¹, B. Gómez⁸, A. Goussiou⁸², P.D. Grannis⁷², H. Greenlee⁵⁰, Z.D. Greenwood⁶⁰, E.M. Gregores⁴, G. Grenier²⁰, Ph. Gris¹³, J.-F. Grivaz¹⁶, A. Grohsjean²⁵, S. Grünenwald⁵⁰, M.W. Grünewald³⁰, F. Guo⁷², J. Guo⁷², G. Gutierrez⁵⁰, P. Gutierrez⁷⁵, A. Haas⁷⁰, N.J. Hadley⁶¹, P. Haefner²⁵, S. Hagopian⁴⁹, J. Haley⁶⁸, I. Hall⁶⁵, R.E. Hall⁴⁷, L. Han⁷, K. Harder⁴⁴, A. Harel⁷¹, J.M. Hauptman⁵⁷, R. Hauser⁶⁵, J. Hays⁴³, T. Hebbeker²¹, D. Hedin⁵², J.G. Hegeman³⁴, A.P. Heinson⁴⁸, U. Heintz⁶², C. Hensel^{22,d}, K. Herner⁷², G. Hesketh⁶³, M.D. Hildreth⁵⁵, R. Hirosky⁸¹, J.D. Hobbs⁷², B. Hoeneisen¹², H. Hoeth²⁶, M. Hohlfeld²², S. Hossain⁷⁵, P. Houben³⁴, Y. Hu⁷², Z. Hubacek¹⁰, V. Hynek⁹, I. Iashvili⁶⁹, R. Illingworth⁵⁰, A.S. Ito⁵⁰, S. Jabeen⁶², M. Jaffré¹⁶, S. Jain⁷⁵, K. Jakobs²³, C. Jarvis⁶¹, R. Jesik⁴³, K. Johns⁴⁵, C. Johnson⁷⁰, M. Johnson⁵⁰, A. Jonckheere⁵⁰, P. Jonsson⁴³, A. Juste⁵⁰, E. Kajfasz¹⁵, J.M. Kalk⁶⁰, D. Karmanov³⁸, P.A. Kasper⁵⁰, I. Katsanos⁷⁰, D. Kau⁴⁹, V. Kaushik⁷⁸, R. Kehoe⁷⁹, S. Kermiche¹⁵, N. Khalatyan⁵⁰, A. Khanov⁷⁶, A. Kharchilava⁶⁹, Y.M. Kharzeev³⁶, D. Khatidze⁷⁰, T.J. Kim³¹, M.H. Kirby⁵³, M. Kirsch²¹, B. Klíma⁵⁰, J.M. Kohli²⁷, J.-P. Konrath²³, A.V. Kozelov³⁹, J. Kraus⁶⁵, T. Kuhl²⁴, A. Kumar⁶⁹, A. Kupco¹¹, T. Kurča²⁰, V.A. Kuzmin³⁸, J. Kvita⁹, F. Lacroix¹³, D. Lam⁵⁵, S. Lammers⁷⁰, G. Landsberg⁷⁷, P. Lebrun²⁰, W.M. Lee⁵⁰, A. Leflat³⁸, J. Lellouch¹⁷, J. Li^{78,‡}, L. Li⁴⁸, Q.Z. Li⁵⁰, S.M. Lietti⁵, J.K. Lim³¹, J.G.R. Lima⁵², D. Lincoln⁵⁰, J. Linnemann⁶⁵, V.V. Lipaev³⁹, R. Lipton⁵⁰, Y. Liu⁷, Z. Liu⁶, A. Lobodenko⁴⁰, M. Lokajicek¹¹, P. Love⁴², H.J. Lubatti⁸², R. Luna³, A.L. Lyon⁵⁰, A.K.A. Maciel², D. Mackin⁸⁰, R.J. Madaras⁴⁶, P. Mättig²⁶, C. Magass²¹, A. Magerkurth⁶⁴, P.K. Mal⁸², H.B. Malbouisson³, S. Malik⁶⁷, V.L. Malyshev³⁶, H.S. Mao⁵⁰, Y. Maravin⁵⁹, B. Martin¹⁴, R. McCarthy⁷², A. Melnitchouk⁶⁶, L. Mendoza⁸, P.G. Mercadante⁵, M. Merkin³⁸, K.W. Merritt⁵⁰, A. Meyer²¹, J. Meyer^{22,d}, T. Millet²⁰, J. Mitrevski⁷⁰, R.K. Mommsen⁴⁴, N.K. Mondal²⁹, R.W. Moore⁶, T. Moulik⁵⁸, G.S. Muanza²⁰, M. Mulhearn⁷⁰, O. Mundal²², L. Mundim³, E. Nagy¹⁵, M. Naimuddin⁵⁰, M. Narain⁷⁷, N.A. Naumann³⁵, H.A. Neal⁶⁴, J.P. Negret⁸, P. Neustroev⁴⁰, H. Nilsen²³, H. Nogima³, S.F. Novaes⁵, T. Nunnemann²⁵, V. O'Dell⁵⁰, D.C. O'Neil⁶, G. Obrant⁴⁰, C. Ochando¹⁶, D. Onoprienko⁵⁹, N. Oshima⁵⁰, N. Osman⁴³, J. Osta⁵⁵, R. Otec¹⁰, G.J. Otero y Garzón⁵⁰, M. Owen⁴⁴, P. Padley⁸⁰, M. Pangilinan⁷⁷, N. Parashar⁵⁶, S.-J. Park^{22,d}, S.K. Park³¹, J. Parsons⁷⁰, R. Partridge⁷⁷, N. Parua⁵⁴, A. Patwa⁷³, G. Pawloski⁸⁰, B. Penning²³, M. Perfilov³⁸, K. Peters⁴⁴, Y. Peters²⁶, P. Pétroff¹⁶, M. Petteni⁴³, R. Piegaia¹, J. Piper⁶⁵, M.-A. Pleier²², P.L.M. Podesta-Lerma^{33,c},

V.M. Podstavkov⁵⁰, Y. Pogorelov⁵⁵, M.-E. Pol², P. Polozov³⁷, B.G. Pope⁶⁵, A.V. Popov³⁹, C. Potter⁶, W.L. Prado da Silva³, H.B. Prosper⁴⁹, S. Protopopescu⁷³, J. Qian⁶⁴, A. Quadt^{22,d}, B. Quinn⁶⁶, A. Rakitine⁴², M.S. Rangel², K. Ranjan²⁸, P.N. Ratoff⁴², P. Renkel⁷⁹, S. Reucroft⁶³, P. Rich⁴⁴, J. Rieger⁵⁴, M. Rijssenbeek⁷², I. Ripp-Baudot¹⁹, F. Rizatdinova⁷⁶, S. Robinson⁴³, R.F. Rodrigues³, M. Rominsky⁷⁵, C. Royon¹⁸, P. Rubinov⁵⁰, R. Ruchti⁵⁵, G. Safronov³⁷, G. Sajot¹⁴, A. Sánchez-Hernández³³, M.P. Sanders¹⁷, B. Sanghi⁵⁰, G. Savage⁵⁰, L. Sawyer⁶⁰, T. Scanlon⁴³, D. Schaile²⁵, R.D. Schamberger⁷², Y. Scheglov⁴⁰, H. Schellman⁵³, T. Schliephake²⁶, S. Schlobohm⁸², C. Schwanenberger⁴⁴, A. Schwartzman⁶⁸, R. Schwienhorst⁶⁵, J. Sekaric⁴⁹, H. Severini⁷⁵, E. Shabalina⁵¹, M. Shamim⁵⁹, V. Shary¹⁸, A.A. Shchukin³⁹, R.K. Shivpuri²⁸, V. Siccardi¹⁹, V. Simak¹⁰, V. Sirotenko⁵⁰, P. Skubic⁷⁵, P. Slattery⁷¹, D. Smirnov⁵⁵, G.R. Snow⁶⁷, J. Snow⁷⁴, S. Snyder⁷³, S. Söldner-Rembold⁴⁴, L. Sonnenschein¹⁷, A. Sopczak⁴², M. Sosebee⁷⁸, K. Soustruznik⁹, B. Spurlock⁷⁸, J. Stark¹⁴, J. Steele⁶⁰, V. Stolin³⁷, D.A. Stoyanova³⁹, J. Strandberg⁶⁴, S. Strandberg⁴¹, M.A. Strang⁶⁹, E. Strauss⁷², M. Strauss⁷⁵, R. Ströhmer²⁵, D. Strom⁵³, L. Stutte⁵⁰, S. Sumowidagdo⁴⁹, P. Svoisky⁵⁵, A. Sznajder³, P. Tamburello⁴⁵, A. Tanasijczuk¹, W. Taylor⁶, B. Tiller²⁵, F. Tissandier¹³, M. Titov¹⁸, V.V. Tokmenin³⁶, I. Torchiani²³, D. Tsybychev⁷², B. Tuchming¹⁸, C. Tully⁶⁸, P.M. Tuts⁷⁰, R. Unalan⁶⁵, L. Uvarov⁴⁰, S. Uvarov⁴⁰, S. Uzunyan⁵², B. Vachon⁶, P.J. van den Berg³⁴, R. Van Kooten⁵⁴, W.M. van Leeuwen³⁴, N. Varelas⁵¹, E.W. Varnes⁴⁵, I.A. Vasilyev³⁹, M. Vaupel²⁶, P. Verdier²⁰, L.S. Vertogradov³⁶, M. Verzocchi⁵⁰, D. Vilanova¹⁸, F. Villeneuve-Seguier⁴³, P. Vint⁴³, P. Vokac¹⁰, E. Von Toerne⁵⁹, M. Voutilainen^{68,e}, R. Wagner⁶⁸, H.D. Wahl⁴⁹, L. Wang⁶¹, M.H.L.S. Wang⁵⁰, J. Warchol⁵⁵, G. Watts⁸², M. Wayne⁵⁵, G. Weber²⁴, M. Weber^{50,f}, L. Welty-Rieger⁵⁴, A. Wenger^{23,g}, N. Wermes²², M. Wetstein⁶¹, A. White⁷⁸, D. Wicke²⁶, G.W. Wilson⁵⁸, S.J. Wimpenny⁴⁸, M. Wobisch⁶⁰, D.R. Wood⁶³, T.R. Wyatt⁴⁴, Y. Xie⁷⁷, S. Yacoob⁵³, R. Yamada⁵⁰, W.-C. Yang⁴⁴, T. Yasuda⁵⁰, Y.A. Yatsunenko³⁶, H. Yin⁷, K. Yip⁷³, H.D. Yoo⁷⁷, S.W. Youn⁵³, J. Yu⁷⁸, C. Zeitnitz²⁶, S. Zelitch⁸¹, T. Zhao⁸², B. Zhou⁶⁴, J. Zhu⁷², M. Zielinski⁷¹, D. Ziemińska⁵⁴, A. Ziemiński^{54,‡}, L. Zivkovic⁷⁰, V. Zutshi⁵², and E.G. Zverev³⁸

(*The DØ Collaboration*)

¹Universidad de Buenos Aires, Buenos Aires, Argentina

²LAFEX, Centro Brasileiro de Pesquisas Físicas, Rio de Janeiro, Brazil

³Universidade do Estado do Rio de Janeiro, Rio de Janeiro, Brazil

⁴Universidade Federal do ABC, Santo André, Brazil

⁵Instituto de Física Teórica, Universidade Estadual Paulista, São Paulo, Brazil

⁶University of Alberta, Edmonton, Alberta, Canada,

Simon Fraser University, Burnaby, British Columbia,
Canada, York University, Toronto, Ontario, Canada,
and McGill University, Montreal, Quebec, Canada

⁷University of Science and Technology of China, Hefei, People's Republic of China

⁸Universidad de los Andes, Bogotá, Colombia

⁹Center for Particle Physics, Charles University, Prague, Czech Republic

¹⁰Czech Technical University, Prague, Czech Republic

¹¹Center for Particle Physics, Institute of Physics,

Academy of Sciences of the Czech Republic, Prague, Czech Republic

¹²Universidad San Francisco de Quito, Quito, Ecuador

¹³LPC, Université Blaise Pascal, CNRS/IN2P3, Clermont, France

¹⁴LPSC, Université Joseph Fourier Grenoble 1, CNRS/IN2P3,
Institut National Polytechnique de Grenoble, Grenoble, France

¹⁵CPPM, Aix-Marseille Université, CNRS/IN2P3, Marseille, France

¹⁶LAL, Université Paris-Sud, IN2P3/CNRS, Orsay, France

¹⁷LPNHE, IN2P3/CNRS, Universités Paris VI and VII, Paris, France

¹⁸CEA, Irfu, SPP, Saclay, France

¹⁹IPHC, Université Louis Pasteur, CNRS/IN2P3, Strasbourg, France

²⁰IPNL, Université Lyon 1, CNRS/IN2P3, Villeurbanne, France and Université de Lyon, Lyon, France

²¹III. Physikalisches Institut A, RWTH Aachen University, Aachen, Germany

²²Physikalisches Institut, Universität Bonn, Bonn, Germany

²³Physikalisches Institut, Universität Freiburg, Freiburg, Germany

²⁴Institut für Physik, Universität Mainz, Mainz, Germany

²⁵Ludwig-Maximilians-Universität München, München, Germany

²⁶Fachbereich Physik, University of Wuppertal, Wuppertal, Germany

²⁷Punjabi University, Chandigarh, India

²⁸Delhi University, Delhi, India

²⁹Tata Institute of Fundamental Research, Mumbai, India

- ³⁰University College Dublin, Dublin, Ireland
³¹Korea Detector Laboratory, Korea University, Seoul, Korea
³²SungKyunKwan University, Suwon, Korea
³³CINVESTAV, Mexico City, Mexico
³⁴FOM-Institute NIKHEF and University of Amsterdam/NIKHEF, Amsterdam, The Netherlands
³⁵Radboud University Nijmegen/NIKHEF, Nijmegen, The Netherlands
³⁶Joint Institute for Nuclear Research, Dubna, Russia
³⁷Institute for Theoretical and Experimental Physics, Moscow, Russia
³⁸Moscow State University, Moscow, Russia
³⁹Institute for High Energy Physics, Protvino, Russia
⁴⁰Petersburg Nuclear Physics Institute, St. Petersburg, Russia
⁴¹Lund University, Lund, Sweden, Royal Institute of Technology and Stockholm University, Stockholm, Sweden, and Uppsala University, Uppsala, Sweden
⁴²Lancaster University, Lancaster, United Kingdom
⁴³Imperial College, London, United Kingdom
⁴⁴University of Manchester, Manchester, United Kingdom
⁴⁵University of Arizona, Tucson, Arizona 85721, USA
⁴⁶Lawrence Berkeley National Laboratory and University of California, Berkeley, California 94720, USA
⁴⁷California State University, Fresno, California 93740, USA
⁴⁸University of California, Riverside, California 92521, USA
⁴⁹Florida State University, Tallahassee, Florida 32306, USA
⁵⁰Fermi National Accelerator Laboratory, Batavia, Illinois 60510, USA
⁵¹University of Illinois at Chicago, Chicago, Illinois 60607, USA
⁵²Northern Illinois University, DeKalb, Illinois 60115, USA
⁵³Northwestern University, Evanston, Illinois 60208, USA
⁵⁴Indiana University, Bloomington, Indiana 47405, USA
⁵⁵University of Notre Dame, Notre Dame, Indiana 46556, USA
⁵⁶Purdue University Calumet, Hammond, Indiana 46323, USA
⁵⁷Iowa State University, Ames, Iowa 50011, USA
⁵⁸University of Kansas, Lawrence, Kansas 66045, USA
⁵⁹Kansas State University, Manhattan, Kansas 66506, USA
⁶⁰Louisiana Tech University, Ruston, Louisiana 71272, USA
⁶¹University of Maryland, College Park, Maryland 20742, USA
⁶²Boston University, Boston, Massachusetts 02215, USA
⁶³Northeastern University, Boston, Massachusetts 02115, USA
⁶⁴University of Michigan, Ann Arbor, Michigan 48109, USA
⁶⁵Michigan State University, East Lansing, Michigan 48824, USA
⁶⁶University of Mississippi, University, Mississippi 38677, USA
⁶⁷University of Nebraska, Lincoln, Nebraska 68588, USA
⁶⁸Princeton University, Princeton, New Jersey 08544, USA
⁶⁹State University of New York, Buffalo, New York 14260, USA
⁷⁰Columbia University, New York, New York 10027, USA
⁷¹University of Rochester, Rochester, New York 14627, USA
⁷²State University of New York, Stony Brook, New York 11794, USA
⁷³Brookhaven National Laboratory, Upton, New York 11973, USA
⁷⁴Langston University, Langston, Oklahoma 73050, USA
⁷⁵University of Oklahoma, Norman, Oklahoma 73019, USA
⁷⁶Oklahoma State University, Stillwater, Oklahoma 74078, USA
⁷⁷Brown University, Providence, Rhode Island 02912, USA
⁷⁸University of Texas, Arlington, Texas 76019, USA
⁷⁹Southern Methodist University, Dallas, Texas 75275, USA
⁸⁰Rice University, Houston, Texas 77005, USA
⁸¹University of Virginia, Charlottesville, Virginia 22901, USA and
⁸²University of Washington, Seattle, Washington 98195, USA

(Dated: July 21, 2008)

We present a measurement of the electron charge asymmetry in $p\bar{p} \rightarrow W + X \rightarrow e\nu + X$ events at a center of mass energy of 1.96 TeV using 0.75 fb^{-1} of data collected with the D0 detector at the Fermilab Tevatron Collider. The asymmetry is measured as a function of the electron transverse momentum and pseudorapidity in the interval $(-3.2, 3.2)$ and is compared with expectations from next-to-leading order calculations in perturbative quantum chromodynamics. These measurements will allow more accurate determinations of the proton parton distribution functions.

PACS numbers: 13.38.Be, 13.85.Qk, 14.60.Cd, 14.70.Fm

In proton-antiproton scattering, W^+ (W^-) bosons are produced primarily by the annihilation of u (d) quarks in the proton with \bar{d} (\bar{u}) quarks in the antiproton. Any difference between the u - and d -quark parton distribution functions (PDFs) will result in an asymmetry in the W boson rapidity distribution between W^+ and W^- boson production. In this Letter we present a new measurement of this asymmetry with much larger statistical precision and over a wider kinematic range than previous measurements [1, 2]. This information provides improved constraints on the PDFs, which should lead not only to reduced theoretical uncertainties in precision determinations of the W boson mass, but also predictions for the Higgs boson production at the Tevatron and at future hadron colliders. Throughout this Letter, we use the notation “electron” to mean “electron and positron”, unless specified otherwise.

We detect W bosons via their decay $W \rightarrow e\nu$. The boson rapidity (y_W) can not be measured due to the unknown longitudinal momentum of the neutrino. We instead measure the electron charge asymmetry, which is a convolution of the W boson production asymmetry and the parity violating asymmetry from the W boson decay. Since the $V-A$ interaction is well understood, the lepton charge asymmetry retains sensitivity to the underlying W boson asymmetry. The electron charge asymmetry ($A(\eta^e)$) is defined as:

$$A(\eta^e) = \frac{d\sigma^+/d\eta^e - d\sigma^-/d\eta^e}{d\sigma^+/d\eta^e + d\sigma^-/d\eta^e}, \quad (1)$$

where η^e is the pseudorapidity of the electron [3] and $d\sigma^+/d\eta^e$ ($d\sigma^-/d\eta^e$) is the differential cross section for the electrons from W^+ (W^-) bosons as a function of the electron pseudorapidity. When the detection efficiencies and acceptances for positrons and electrons are identical, the asymmetry becomes the difference in the number of positron and electron events over the sum, and some systematic uncertainties on these quantities do not affect $A(\eta^e)$.

In this Letter we present results obtained from more than twice the integrated luminosity of previous measurements by the CDF [1] and D0 [2] collaborations and extend the measurement for leptons with $|\eta^\ell| < 3.2$, compared to $|\eta^\ell| < 2.5$ for CDF and $|\eta^\ell| < 2.0$ for the previous D0 measurement. By extending to higher rapidity leptons, we can provide information about the PDFs for a broader x range ($0.002 < x < 1.0$ for $|y_W| < 3.2$) at high $Q^2 \sim M_W^2$, where Q^2 is the momentum transfer squared, x is the fraction of momentum of the proton carried by the parton and M_W is the W boson mass.

The data sample used in this measurement was collected with the D0 detector [4] at the Fermilab Tevatron Collider using a set of inclusive single-electron triggers based only on calorimeter information. The integrated luminosity is $750 \pm 46 \text{ pb}^{-1}$ [5].

The D0 detector includes a central tracking system, composed of a silicon microstrip tracker (SMT) and a central fiber tracker (CFT), both located within a 2 T superconducting solenoidal magnet and covering pseudorapidities of $|\eta_D| < 3.0$ and $|\eta_D| < 2.5$ respectively [3]. Three liquid argon and uranium calorimeters provide coverage out to $|\eta_D| \approx 4.2$: a central section (CC) with coverage of $|\eta_D| < 1.1$ and two end calorimeters (EC) with a coverage of $1.5 < |\eta_D| < 4.2$. All three sections are longitudinally segmented into electromagnetic and hadronic parts respectively.

W boson candidates are identified by one isolated electromagnetic cluster accompanied by large missing transverse energy (\cancel{E}_T). \cancel{E}_T is determined by the vector sum of the transverse components of the energy deposited in the calorimeter and the transverse momentum (E_T) of the electron. Electron candidates are further required to have shower shapes consistent with that of an electron. The E_T of the electron and the \cancel{E}_T are required to be greater than 25 GeV. Additionally, the transverse mass M_T of the electron and \cancel{E}_T is required to be greater than 50 GeV, where $M_T = \sqrt{2E_T\cancel{E}_T(1 - \cos\Delta\phi)}$, and $\Delta\phi$ is the azimuthal angle between the electron and \cancel{E}_T .

Electrons are required to fall within the fiducial region of the calorimeters, and must be spatially matched to a reconstructed track in the central tracking system. Because of the different geometrical coverage of the calorimeters and the tracker, the electrons are divided into four different types depending on the locations of the electrons in the calorimeter and the associated track polar angle and the collision vertex: CC electrons within the full coverage of the CFT, EC electrons within the full coverage of the CFT, EC electrons within the partial coverage of the CFT, and EC electrons outside the coverage of the CFT. Optimized choices for selection criteria are established for each type. A total of 491,250 events satisfy the selection, with 358,336 events with electrons in the CC and 132,914 events with electrons in the EC. The charge asymmetry is measured in 24 electron pseudorapidity bins for $|\eta^e| < 3.2$.

The asymmetry measurement is sensitive to misidentification of the electron charge. We measure the charge misidentification rate with $Z \rightarrow ee$ events using a “tag-and-probe” method [6] where a track matched to one electron tags the charge of the other. Tight conditions are applied on the tag electron to make sure its charge is correctly determined. The result from the tag-and-probe method is corroborated using the fraction of same-sign events observed in data in the Z boson pole region. The rate ranges from 0.2% at $|\eta^e| \approx 0$ to 9% at $|\eta^e| \approx 3$. The absolute uncertainty in the charge misidentification changes from 0.1% to 2.6% depending on the electron pseudorapidity, and is dominated by the statistics of the Z boson sample.

Sources of charge bias in the event selection are investigated by studying $Z \rightarrow ee$ events. All selection efficien-

cies are measured for electrons and positrons separately, and no charge dependent biases in acceptance or efficiencies are found. To reduce any possible residual charge determination biases due to instrumental effects, the direction of the magnetic field in the solenoidal magnet was regularly reversed. Approximately 46% of the selected W bosons were collected with the solenoid at forward polarity, and 54% at reverse polarity. The charge asymmetry is measured separately for each solenoid polarity and no significant differences are observed.

Three sources of background can dilute the charge asymmetry: $Z \rightarrow ee$ events where one electron is not detected by the calorimeter, $W \rightarrow \tau\nu \rightarrow e\nu\nu\nu$ events, and multijet events in which one jet is misidentified as an electron and a large \cancel{E}_T is produced by fragmentation fluctuations or misreconstruction. The $A(\eta^e)$ values are corrected for the backgrounds in each bin.

Events with electrons from $Z \rightarrow ee$ and $W \rightarrow \tau\nu \rightarrow e\nu\nu\nu$ decays exhibit charge asymmetries, and these two background contributions are evaluated using Monte Carlo (MC) events generated with PYTHIA [7] and processed with a detailed detector simulation based on GEANT [8]. The fractions of $Z \rightarrow ee$ and $W \rightarrow \tau\nu \rightarrow e\nu\nu\nu$ events estimated to contribute to the candidate sample are $(1.3 \pm 0.1)\%$ and $(2.1 \pm 0.1)\%$, respectively.

The background fraction from multijet events is estimated by starting from a sample of candidate events with loose shower shape requirements and then selecting a subset of events which satisfy the final tighter requirement. From $Z \rightarrow ee$ events, and a sample of multijet events passing the preselection but with low \cancel{E}_T , we determine the probabilities with which real and fake electrons will pass the final shower shape requirement. These two probabilities (verified to be charge symmetric), along with the number of events selected in the loose and tight samples allow us to calculate the fraction of multijet events within our final selection. The final background contamination from multijet events is estimated to be $(0.8 \pm 0.4)\%$.

The final charge asymmetry is corrected for electron energy scale and resolution, \cancel{E}_T resolution and trigger efficiency. The correction is estimated by comparing the asymmetry from the generator level PYTHIA $W \rightarrow e\nu$ MC to the GEANT-simulated results for each electron type.

The electron charge asymmetry is determined separately for each electron pseudorapidity bin and for each of the four electron types and then combined. The charge misidentification and background estimations are performed independently for each of these measurements. Assuming $A(-\eta^e) = -A(\eta^e)$ due to CP invariance, we fold the data to increase the available statistics and obtain a more precise measurement of $A(\eta^e)$.

Figure 1 shows the folded electron charge asymmetry. The dominant sources of systematic uncertainties originate from the estimation of charge misidentification and multijet backgrounds. The bin-by-bin correlations of these systematic uncertainties are negligible. Also

shown in Fig. 1 are the theoretical predictions obtained using the RESBOS event generator [9] (with gluon resummation at low boson p_T and NLO perturbative QCD calculations at high boson p_T) with PHOTOS [10] (for QED final state radiation). The PDFs used to generate these predictions are the CTEQ6.6 NLO PDFs [11] and MRST04NLO PDFs [13]. Theoretical uncertainties derived from the 44 CTEQ6.6 PDF uncertainty sets are also shown. These curves are generated by applying a 25 GeV cut on the electron and neutrino generator-level transverse momenta. The asymmetric PDF uncertainty band is calculated using the formula described in Ref. [12].

We also measure the asymmetry in two bins of electron E_T : $25 < E_T < 35$ GeV and $E_T > 35$ GeV. For a given η^e , the two E_T regions probe different ranges of y_W and thus allow a finer probe of the x dependence. The folded electron charge asymmetries, along with the theoretical predictions, for the two electron E_T bins are shown in Fig. 2.

The measured values of the asymmetry and uncertainties, together with the CTEQ6.6 predictions, for $E_T > 25$ GeV and the two separate E_T bins are listed in Table I. The measured charge asymmetries tend to be lower than the theoretical predictions using both CTEQ6.6 central PDF set and MRST04NLO PDFs for high pseudorapidity electrons. For most η^e bins, the experimental uncertainties are smaller than the uncertainties given by the most recent CTEQ6.6 uncertainty sets, demonstrating the sensitivity of our measurement.

In summary, we have measured the charge asymmetry of electrons in $p\bar{p} \rightarrow W + X \rightarrow e\nu + X$ using 0.75 fb^{-1} of data. The electron coverage is extended to $|\eta^e| < 3.2$ and the asymmetry is measured for electron $E_T > 25$ GeV, as well as two separate E_T bins to improve sensitivity to the PDFs. This measurement is the most precise electron charge asymmetry measurement to date, and the experimental uncertainties are smaller than the theoretical uncertainties across almost all electron pseudorapidities. Our result can be used to improve the precision and accuracy of next generation PDF sets, and will help to reduce the PDF uncertainty for high precision M_W measurements and also improve the predictions for the Higgs boson production at the hadron colliders.

We thank P. Nadolsky for many useful discussions about the theoretical predictions. We thank the staffs at Fermilab and collaborating institutions, and acknowledge support from the DOE and NSF (USA); CEA and CNRS/IN2P3 (France); FASI, Rosatom and RFBR (Russia); CNPq, FAPERJ, FAPESP and FUNDUNESP (Brazil); DAE and DST (India); Colciencias (Colombia); CONACyT (Mexico); KRF and KOSEF (Korea); CONICET and UBACyT (Argentina); FOM (The Netherlands); STFC (United Kingdom); MSMT and GACR (Czech Republic); CRC Program, CFI, NSERC and WestGrid Project (Canada); BMBF and DFG (Germany); SFI (Ireland); The Swedish Research Council

η^e region	$\langle \eta^e \rangle$	$A(\eta^e)$					
		$E_T > 25$ GeV		$25 < E_T < 35$ GeV		$E_T > 35$ GeV	
		Data	Prediction	Data	Prediction	Data	Prediction
0.0 – 0.2	0.10	$1.6 \pm 0.4 \pm 0.3$	$1.9^{+0.4}_{-0.5}$	$1.9 \pm 0.6 \pm 0.5$	$2.1^{+0.5}_{-0.8}$	$1.4 \pm 0.5 \pm 0.4$	$1.8^{+0.5}_{-0.7}$
0.2 – 0.4	0.30	$5.6 \pm 0.4 \pm 0.3$	$5.7^{+0.4}_{-1.2}$	$6.8 \pm 0.6 \pm 0.5$	$6.2^{+0.8}_{-1.3}$	$4.8 \pm 0.5 \pm 0.4$	$5.3^{+0.5}_{-1.3}$
0.4 – 0.6	0.50	$8.2 \pm 0.4 \pm 0.3$	$9.1^{+1.2}_{-0.9}$	$9.3 \pm 0.6 \pm 0.5$	$9.8^{+1.2}_{-0.8}$	$7.5 \pm 0.5 \pm 0.4$	$8.5^{+1.3}_{-1.1}$
0.6 – 0.8	0.70	$13.0 \pm 0.4 \pm 0.3$	$12.2^{+1.5}_{-1.2}$	$13.8 \pm 0.6 \pm 0.5$	$12.4^{+3.1}_{-0.3}$	$12.4 \pm 0.5 \pm 0.4$	$12.1^{+1.0}_{-2.3}$
0.8 – 1.0	0.90	$14.6 \pm 0.4 \pm 0.3$	$14.8^{+1.3}_{-1.8}$	$15.8 \pm 0.7 \pm 0.6$	$14.6^{+1.7}_{-1.3}$	$13.9 \pm 0.5 \pm 0.4$	$15.0^{+1.3}_{-2.4}$
1.0 – 1.2	1.10	$15.5 \pm 0.6 \pm 0.5$	$16.6^{+1.0}_{-2.5}$	$15.8 \pm 1.0 \pm 0.8$	$15.2^{+0.7}_{-3.0}$	$15.2 \pm 0.8 \pm 0.6$	$17.6^{+1.5}_{-2.4}$
1.2 – 1.6	1.39	$14.4 \pm 0.6 \pm 0.5$	$16.4^{+1.8}_{-2.2}$	$12.9 \pm 1.0 \pm 0.8$	$11.1^{+1.8}_{-1.8}$	$17.0 \pm 0.8 \pm 0.6$	$20.4^{+2.2}_{-2.6}$
1.6 – 1.8	1.70	$10.2 \pm 0.5 \pm 0.4$	$13.0^{+2.3}_{-2.2}$	$-0.1 \pm 0.8 \pm 0.6$	$0.7^{+3.2}_{-1.3}$	$17.9 \pm 0.6 \pm 0.6$	$21.7^{+2.0}_{-3.1}$
1.8 – 2.0	1.90	$6.6 \pm 0.6 \pm 0.5$	$8.3^{+2.2}_{-3.3}$	$-12.0 \pm 1.0 \pm 0.8$	$-10.1^{+2.2}_{-2.7}$	$19.7 \pm 0.8 \pm 0.7$	$21.2^{+2.7}_{-4.1}$
2.0 – 2.2	2.09	$-2.5 \pm 0.9 \pm 0.6$	$0.9^{+4.3}_{-3.0}$	$-24.7 \pm 1.3 \pm 1.2$	$-23.6^{+4.1}_{-2.2}$	$14.4 \pm 1.2 \pm 0.9$	$18.7^{+4.8}_{-3.9}$
2.2 – 2.6	2.37	$-19.8 \pm 1.0 \pm 0.7$	$-12.0^{+5.1}_{-5.1}$	$-42.9 \pm 1.4 \pm 1.6$	$-39.4^{+3.2}_{-3.3}$	$1.1 \pm 1.4 \pm 0.7$	$12.6^{+7.4}_{-7.5}$
2.6 – 3.2	2.80	$-54.3 \pm 4.2 \pm 4.2$	$-36.1^{+9.4}_{-7.2}$	$-76.2 \pm 5.0 \pm 7.1$	$-55.1^{+6.0}_{-4.3}$	$-14.8 \pm 6.7 \pm 2.6$	$-1.7^{+17.9}_{-14.4}$

TABLE I: Folded electron charge asymmetry for data and predictions from RESBOS with PHOTOS using CTEQ6.6 PDFs tabulated in percent. $\langle |\eta^e| \rangle$ is the cross section weighted average of electron pseudorapidity in each bin from RESBOS with PHOTOS. For data, the first uncertainty is statistical and the second is systematic. For the predictions, the uncertainties are from the PDFs only.

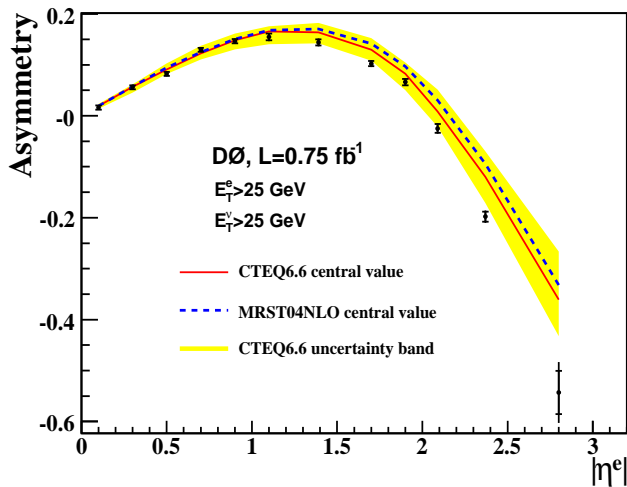


FIG. 1: (color online) The folded electron charge asymmetry distribution. The horizontal bars show the statistical uncertainty and the full vertical lines show the total uncertainty on each point. The solid line is the theoretical prediction for the asymmetry using CTEQ6.6 central PDF set. The dashed line shows the same prediction using the MRST04NLO PDFs. The shaded band is the uncertainty band determined using the 44 CTEQ6.6 PDF uncertainty sets. All three were determined using RESBOS with PHOTOS.

(Sweden); CAS and CNSF (China); and the Alexander von Humboldt Foundation (Germany).

- [a] Visitor from Augustana College, Sioux Falls, SD, USA.
- [b] Visitor from The University of Liverpool, Liverpool, UK.
- [c] Visitor from ECFM, Universidad Autonoma de Sinaloa, Culiacán, Mexico.
- [d] Visitor from II. Physikalisches Institut, Georg-August-University, Göttingen, Germany.
- [e] Visitor from Helsinki Institute of Physics, Helsinki, Finland.
- [f] Visitor from Universität Bern, Bern, Switzerland.
- [g] Visitor from Universität Zürich, Zürich, Switzerland.
- [‡] Deceased.
- [1] F. Abe *et al.* (CDF Collaboration), Phys. Rev. Lett. **74**, 850 (1995); F. Abe *et al.* (CDF Collaboration), Phys. Rev. Lett. **81**, 5754 (1998); D. Acosta *et al.* (CDF Collaboration), Phys. Rev. D **71**, 051104(R) (2005).
- [2] V. Abazov *et al.* (D0 Collaboration), Phys. Rev. D **77**, 011106(R) (2008).
- [3] D0 uses a cylindrical coordinate system with the z axis running along the beam axis in the proton direction. Angles θ and ϕ are the polar and azimuthal angles, respectively. Pseudorapidity is defined as $\eta = -\ln[\tan(\theta/2)]$ where θ is measured with respect to the interaction vertex. In the massless limit, η is equivalent to the rapidity $y = (1/2) \ln[(E + p_z)/(E - p_z)]$. η_D is the pseudorapidity measured with respect to the center of the detector. Due to the distribution of the interactions within the detector, electrons may have larger η than η_D .
- [4] V. Abazov *et al.* (D0 Collaboration), Nucl. Instrum. Methods Phys. Res., Sect. A **565**, 463 (2006).
- [5] T. Andeen *et al.*, FERMILAB-TM-2365 (2007).
- [6] V. Abazov *et al.* (D0 Collaboration), Phys. Rev. D **76**,

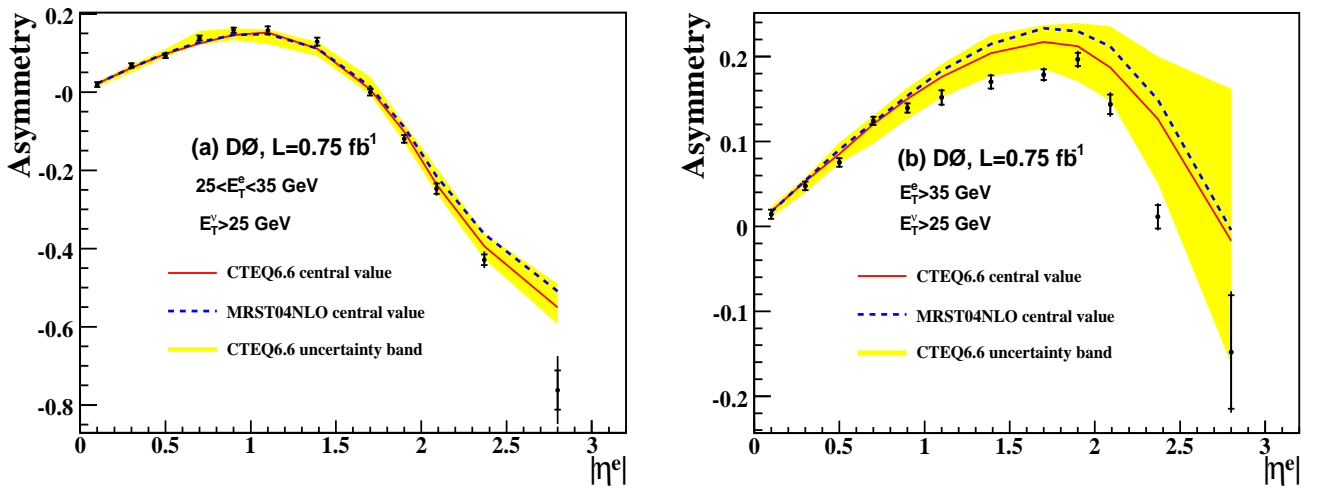


FIG. 2: (color online) The folded electron charge asymmetry distribution in two electron E_T bins: $25 < E_T < 35 \text{ GeV}$ for (a) and $E_T > 35 \text{ GeV}$ for (b). In each plot, the horizontal bars show the statistical uncertainty and the full vertical lines show the total uncertainty on each point. The solid line is the theoretical prediction for the asymmetry using CTEQ6.6 central PDF set. The dashed line shows the same prediction using the MRST04NLO PDF set. The shaded band is the uncertainty band determined using the 44 CTEQ6.6 PDF uncertainty sets. All three were determined using RESBOS with PHOTOS.

- 012003 (2007).
- [7] T. Sjöstrand *et. al.*, Comput. Phys. Commun. **135**, 238 (2001).
 - [8] R. Brun and F. Carminati, CERN Program Library Long Writeup W5013, 1993 (unpublished).
 - [9] C. Balazs and C.P. Yuan, Phys. Rev. D **56**, 5558 (1997).
 - [10] E. Barberio and Z. Was, Comput. Phys. Commun. **79**, 291 (1994); we use PHOTOS version 2.0.
 - [11] P.M. Nadolsky *et al.*, Phys. Rev. D **78**, 013004 (2008).
 - [12] D. Stump *et al.*, JHEP **0310**, 046 (2003).
 - [13] A.D. Martin, R.G. Roberts, W.J. Stirling, and R.S. Thorne, Phys. Lett. B **604**, 61 (2004).